

Evidence of trivalent Am substitution into U₃O₈

Caisso, M.; Roussel, P.; Den Auwer, C.; Picart, S.; Hennig, C.; Scheinost, A. C.;
Delahaye, T.; Ayrat, A.;

Originally published:

September 2016

Inorganic Chemistry 55(2016), 10438-10444

DOI: <https://doi.org/10.1021/acs.inorgchem.6b01672>

Perma-Link to Publication Repository of HZDR:

<https://www.hzdr.de/publications/Publ-24061>

Release of the secondary publication
on the basis of the German Copyright Law § 38 Section 4.

Evidence of trivalent Am substitution into U₃O₈

Marie Caisso^{1,2,7}, Pascal Roussel³, Christophe Den Auwer⁴, Sébastien Picart², Christoph Hennig⁵, Andreas C. Scheinost^{5,6}, Thibaud Delahaye^{2,}, André Ayrat⁷*

¹CEA, DEN, DTEC/SECA/LFC, F-30207 Bagnols-sur-Cèze Cedex, France

²CEA, DEN, DRCP/SERA/LCAR, F-30207 Bagnols-sur-Cèze Cedex, France

³Unité de Catalyse et Chimie du Solide, UMR 8012 CNRS, 59652 Villeneuve d'Ascq Cedex, France

⁴Université Nice Sophia Antipolis, Institut de Chimie de Nice, UMR 7272, F-06108 Nice cedex

2

⁵HZDR, Institute of Resource Ecology - 01314 Dresden, Germany

⁶The Rossendorf Beamline at ESRF – 38043 Grenoble, France

⁷Institut Européen des Membranes, UMR 5635 CNRS-ENSCM-UM2, CC047, Université Montpellier 2, F-34095 Montpellier Cedex 5, France

KEYWORDS. U₃O₈, uranium-ameridium mixed oxide, EXAFS, XANES, XRD.

ABSTRACT. U₃O₈ is considered as the most stable phase for uranium oxide, justifying the necessity to precisely know its structural properties in order to apprehend its behavior in storage conditions as regards leaching in the case of spent nuclear fuel storage in oxidative conditions.

1
2
3 Nevertheless, as fuel irradiation causes the formation of fission products and activation products
4 such as plutonium and minor actinides, it is probable that U_3O_8 oxide would be mixed with other
5 chemical elements in real conditions of oxidation. Storage issue can be extended to americium
6 transmutation where compounds dedicated to irradiation are mixed-oxides composed of uranium
7 and americium. Present study is thus focusing on the determination of the structural properties of
8 a solid solution containing uranium and trivalent americium (U/Am ratio = 90/10), and
9 synthesized as to obtain conventional U_3O_8 oxide. It presents for the first time the possibility to
10 combine trivalent americium with uranium as mixed-oxide under U_3O_8 form, despite the high
11 valence and atomic ratio differences, and propose novel structural arrangements. XRD
12 measurements reveal americium substitution in U_3O_8 uranium cationic site, leading to phase
13 transformation to U_3O_8 high temperature structure and general lattice swelling. XANES and
14 EXAFS experiments highlight, as main consequence for accommodation, excess of U^{+VI}
15 organized in uranyl units.
16
17
18
19
20
21
22
23
24
25
26
27
28
29
30
31
32
33

34 35 INTRODUCTION

36
37
38 Oxidation of uranium (U) dioxide (UO_2) into U_3O_8 has been studied for years in the field of
39 nuclear fuel fabrication. It was first considered for nuclear fuel reprocessing, and is now
40 considered in waste management domain and spent fuel behavior in dry storage conditions.^{1,2}
41 Indeed, as UO_2 is the most common uranium form used as nuclear fuel, U_3O_8 is the most stable
42 uranium oxide in ambient conditions, close to the U compounds found in natural environment.
43 Left at room temperature (RT) under air, UO_2 is slowly oxidized into U_3O_8 .³ Focusing on spent
44 fuels, even if major part is still composed of UO_2 , the presence of additional radionuclides with
45 high radioactivity such as fission products or minor actinides (MA) and thus generating heat
46
47
48
49
50
51
52
53
54
55
56
57
58
59
60

1
2
3 load, leads to faster UO_2 oxidation into U_3O_8 , accelerating intermediate phase transformation
4
5 such as U_4O_9 and U_3O_7 .⁴ This issue also concern compounds fabricated in the field of MA
6
7 transmutation,^{5,6} where the latter can be integrated to uranium oxides, to form, in the case of
8
9 americium (Am), dense $\text{U}_{1-x}\text{Am}_x\text{O}_{2\pm\delta}$ pellets. Storage and post-irradiation behavior of these
10
11 compounds under oxidative conditions remain unknown and are identified as crucial factors for
12
13 future experimental irradiation. Furthermore U_3O_8 compound is also used as mineral poreformer
14
15 in nuclear fuel fabrication.^{7,6} Impurity solubility in this oxide should thus be well-known to
16
17 anticipate chemical reaction between U_3O_8 as poreformer and other actinides composing fuels,
18
19 such as MOX fuel^{8,9} or dedicated compounds for transmutation.

20
21
22 Considering first literature on pure U_3O_8 , at RT its crystalline structure was determined as
23
24 orthorhombic (space group $C2mm$) and this form is called $\alpha\text{-U}_3\text{O}_8$.¹⁰⁻¹³ When heated at 483 K, α
25
26 form is converted into α' one with transition to hexagonal space group $P-62m$. This transition
27
28 and the consequent atomic positions modifications were studied by Loopstra et al.¹⁴ and
29
30 Ackermann et al.¹⁵, who defined current space group and positions for U and O in $\alpha\text{-U}_3\text{O}_8$ and α' -
31
32 U_3O_8 forms. If many characterizations have been performed on U_3O_8 to explain crystallographic
33
34 structures,^{10,12,14,16,17} few papers exist on U_3O_8 accommodating with another chemical element.
35
36 Tetravalent Pu and Np were integrated to U_3O_8 to form a solid solution. Benedict et al. report
37
38 some space group change with Pu incorporation,¹⁸ such as Finch et al. for Np,¹⁹ but no structural
39
40 models were presented to explain how these elements present as impurities are accommodated in
41
42 the structure. More recently, Remy synthesized same kind of mixed oxide containing tetravalent
43
44 Ce.²⁰ In the following study, Am was the chosen substituted element, answering transmutation
45
46 target research need for post-irradiation characterizations. Mixed oxides composed of U and Am
47
48 were synthesized under oxidative atmosphere, in the same conditions required for U_3O_8
49
50
51
52
53
54
55
56
57
58
59
60

1
2
3 formation.^{21–23} Obtained crystalline structure was fully characterized and compared to pure
4 U_3O_8 . To begin, XRD results presenting the new crystalline structure and its difference with the
5
6 pure compound are exposed and analyzed. These results were completed by XANES
7
8 measurements allowing to assess the formal oxidation states of U and Am in the mixed-oxide.
9
10 Finally EXAFS data fitting was used to reconstruct the close environment of the U and Am
11
12 cations and the establishing of metal-O and metal-metal first distances, highlighting what enables
13
14 Am to be substituted in the U_3O_8 structure.
15
16
17
18
19
20
21
22

23 EXPERIMENTAL SECTION

24
25
26 **Sample preparation.** A wet chemical route based on the use on ion exchange resin
27
28 microspheres was selected in this work to ensure in the final oxide a homogeneous repartition of
29
30 actinide element at the atomic scale. This process of (U,Am) based samples was the same as
31
32 described in previous works for actinide based mixed-oxide synthesis.^{22,23} Stoichiometric
33
34 amounts of uranyl and americium cations dissolved in aqueous solution, implying the following
35
36 atomic U/Am ratio of 90/10, were fixed on the exchanger sites of weak acid resin (WAR)
37
38 microspheres, releasing proton ions. After complete exchange (stable pH of the solution), loaded
39
40 resin was extracted and dried at 373 K. Microspheres were finally calcined for 4 h at 973 K
41
42 under air, following a heating rate of 5 K.min⁻¹. This calcination was performed in a tubular
43
44 furnace (Lenton LTF), in which microspheres were disposed as a single layer in a quartz
45
46 crucible. The same protocol was followed for pure U_3O_8 reference microspheres.
47
48
49
50
51

52
53 **X-Ray Diffraction.** RT XRD diagrams were recorded on powdered microspheres using a
54
55 Bruker D8 Advance apparatus equipped with a Cu $K\alpha_{1,2}$ radiation and a linear Lynx-Eye
56
57 detector, in a θ - θ Bragg–Brentano configuration. The step was approximately fixed at 0.02° with
58
59
60

1
2
3 a time per step of 0.3 s, for an angular domain of 15 to 110° 2 θ . Bruker EVA DIFFRACplus
4 software was used for phase identification. Lattice parameters of synthesized compounds were
5
6 determined using the Jana Suite software,^{24,25} with a Le Bail method for refinements.²⁶ A
7
8 pseudo-Voigt profile function was used for lattice parameter refinement. Gold reference was
9
10 added to the powdered sample for position calibrations. The Au phase profile was also fitted but
11
12 lattice parameters were kept fixed as it is used as a reference.
13
14
15

16
17 **XAS experiments.** XAS experiments were carried out at the European Synchrotron Radiation
18 Facility (ESRF, Grenoble, France) on the Rossendorf Beamline (ROBL) with the storage ring
19
20 operating at 6.0 GeV and 170–200 mA. The synchrotron beam was collimated with a 1.3 m long,
21
22 Rh-coated, meridionally-bent mirror, monochromatized with a double-crystal monochromator
23
24 with a water-cooled Si (111) crystal pair, and focalized with a 1.2 long, Rh-coated toroidal
25
26 mirror. XANES spectra were collected in transmission mode at the Am L_{III} (18510 eV) and the
27
28 U L_{III} edge (17166 eV) with a step size of 0.7 eV using ionization chambers. EXAFS
29
30 measurements were performed in both transmission and fluorescence modes, at the Am L_{III}
31
32 (18510 eV) and U L_{II} (20948 eV) edges for Am-substituted U₃O₈ microspheres, and U L_{III} edge
33
34 for pure U₃O₈ microspheres. The use of the U L_{II} edge was necessary because of the presence of
35
36 neptunium impurities in Am, with its L_{III} absorption edge interfering with the U L_{III} EXAFS
37
38 region. The fluorescence signal was measured with a 13-element Ge solid-state detector using a
39
40 digital spectrometer (XIA-XMap). Metallic foils with K edges close to the edges of interest, i.e.
41
42 Y (17038 eV), Zr (17998 eV), and Mo (20000 eV), were used as references for energy
43
44 calibration. EXAFS spectra were recorded at Am L_{III}, U L_{II} and U L_{III} edges, up to k = 18, 13.5
45
46 and 16 Å⁻¹, respectively. During all the measurements, a He cryostat was used to maintain a
47
48 sample temperature around 15 K. The thermal contribution to the Debye-Waller factors is thus
49
50
51
52
53
54
55
56
57
58
59
60

1
2
3 greatly reduced and only the static structural disorder contribution remains. Data refinements
4
5 were performed using the IFEFFIT^{27,28} software and FEFF9²⁹ for ab initio calculations of
6
7 EXAFS spectra. XANES spectra were normalized using a linear function for pre- and post-edge
8
9 approximation. E_0 was arbitrarily assigned to the edge inflection point, determined as the knot of
10
11 the first derivative. U L_{III} edge spectra were compared to that of a UO₃ compound also recorded
12
13 at ROBL under the same conditions, while the Am L_{III} spectra were compared to those of AmO₂
14
15 and pure Am oxalate,³⁰ as Am^{+IV} and Am^{+III} references respectively. Considering the pure U₃O₈
16
17 reference, Fourier transform of the EXAFS spectrum (in k²) was performed with a Hanning
18
19 window between 2.2 and 16 Å⁻¹. For the Am-substituted U₃O₈, Fourier transform of the EXAFS
20
21 spectra (in k²) was performed with a Hanning window between 3 and 13 Å⁻¹ and 3.5 and 2.8 and
22
23 11.8 Å⁻¹ for U L_{II} and Am L_{III} edges respectively. A 7.5 Å-cluster of U₃O₈ was considered for
24
25 data fitting, using the lattice parameters determined through XRD measurements. Model U₃O₈
26
27 was fitted with C2mm space group. In this crystallographic structure, U is coordinated by two
28
29 axial O, 5 equatorial O, 2 axial U and 4 equatorial U as nearest neighbors. Multiple scattering
30
31 along axial directions was taken into account through the addition of triple scattering (U₁-O₂-O_X-
32
33 U₁) and quadruple scattering (U₁-O₂-U_X-O₂-U₁). The structural parameters of the multiple
34
35 scattering paths were linked to that of corresponding single scattering paths to reduce the number
36
37 of free parameters. Considering Am-substituted U₃O₈, two space groups were tested, *P-3m1* and
38
39 *P-62m*, but only the latter allowed the fit to converge. For *P-62m*, the configuration of single
40
41 scatterings around U is the same as for *C2mm* with a few changes on distances. Consequently
42
43 similar triple and quadruple scattering paths were also added and improved the fit quality, with
44
45 structural parameters linked to the single paths. Debye-Waller factors were found equal to
46
47 0.005(1) and 0.0080 Å², and 0.0200 and 0.0150 Å² for UL_{II} and AmL_{III} edges respectively.
48
49
50
51
52
53
54
55
56
57
58
59
60

RESULTS AND DISCUSSION

The following results present and develop the features of the crystallographic structure obtained after (U,Am) loaded resin thermal conversion under air, performed at 973 K. These novel features are compared to pure U_3O_8 microspheres.

XRD results. XRD recorded diagrams for pure U_3O_8 and Am-based U_3O_8 microspheres are presented in Figure 1 and Figure 2 respectively. For pure U_3O_8 X-Ray phase diagram, phase identification matches with the orthorhombic $C2mm$ crystallographic structure. In the context of uranium oxides, it corresponds to the α - U_3O_8 phase, structure stabilized at RT. Le Bail refinement performed on this recorded diagram gives the following lattice parameters: $a = 6.720(2) \text{ \AA}$; $b = 11.952(2) \text{ \AA}$; $c = 4.146(2) \text{ \AA}$ for a lattice volume of $333.02(1) \text{ \AA}^3$. Refinement parameters are summarized in Table 2 and corresponding plots are presented in Figure 1. Structural values, when compared to literature,^{12,14,15} are relevant of standard α - U_3O_8 phase and validates the synthesis of U_3O_8 compound through thermal conversion of WAR microspheres under air at 973 K.

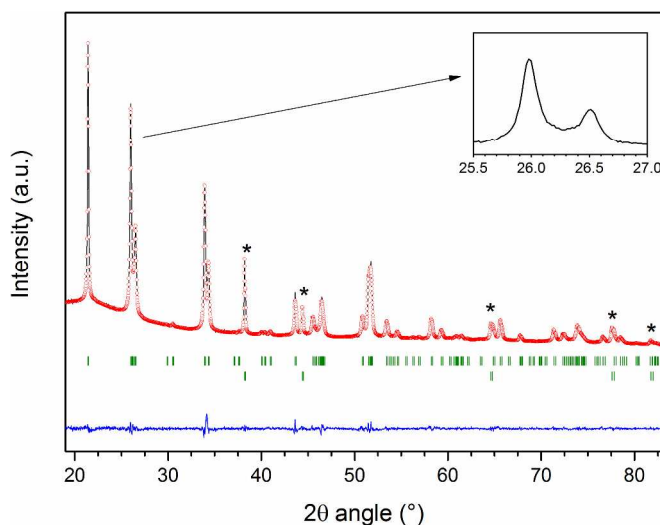
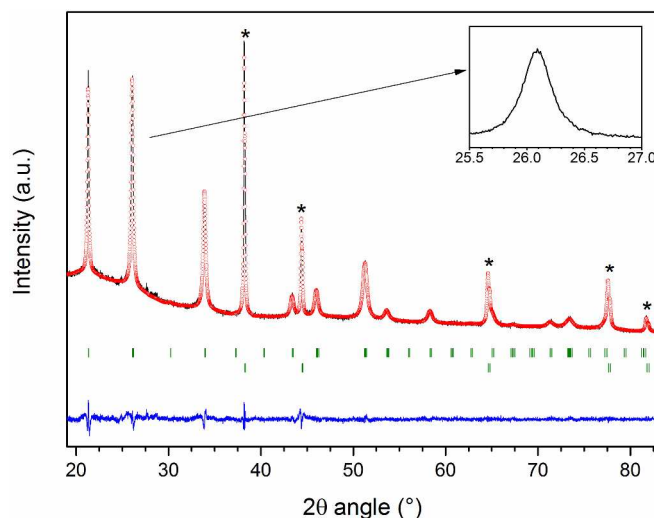


Figure 1. XRD diagram and refinement results of powdered pure U_3O_8 oxide microspheres converted during 4h at 973 K under air – Peak matches with a * correspond to gold phase.

1
2
3 Experimental data is in black; the calculated diagram is in red; the difference between them is in
4
5
6 blue; Bragg positions are presented in green.



26 Figure 2. XRD diagram and refinement results of (U,Am) based oxide microspheres converted
27 during 4h at 973 K under air – Peak matches with a * correspond to gold phase. Experimental
28 data is in black; the calculated diagram is in red for P-62m reference space group; the difference
29 between them is in blue; Bragg positions are presented in green.

30
31
32
33
34
35
36
37 Considering X-Ray diagram collected after thermal conversion of WAR microspheres loaded
38 with U and Am, Figure 2, a diagram associated to a monophasic compound is also obtained after
39 conversion, but if it looks close to that α - U_3O_8 phase, a relevant difference is noticed on the two
40 peaks around 26.5° (enclosed zoom) and 34° . Indeed, pure U_3O_8 phase shows two significant
41 peaks that become merged into a single one in the new phase including Am. About phase
42 identification, two crystallographic structures match with the collected diagram. The first one
43 crystallizes in the trigonal $P-3m1$ space group, taken by α - UO_3 phase,³¹ and the second one in the
44 hexagonal $P-62m$ space group, stabilized at HT (over 500 K) by U_3O_8 .¹⁵ Both own similar
45 cationic sublattice with single cationic position, where differences are undertaken by the O
46
47
48
49
50
51
52
53
54
55
56
57
58
59
60

atoms. In the case of trigonal structure, there are only two O positions, for five positions in hexagonal one, consistent with higher anionic organization in the case of hexagonal structure. The adjustment of crystalline structure with Am presence, through this change of space group, is relevant of Am substitution inside U_3O_8 phase. Le Bail refinements were performed for both possibilities. The lattice parameters determined for $P-62m$ space group, whose refinement is visible in Figure 2, are: $a = 6.838(2) \text{ \AA}$; $c = 4.171(2) \text{ \AA}$ for a total lattice volume of $169.05(1) \text{ \AA}^3$. When refined with $P-3m1$ space group, the following lattice parameters were obtained: $a = 3.948(2) \text{ \AA}$ and $c = 4.167(2) \text{ \AA}$ for a total lattice volume of $56.33(1) \text{ \AA}^3$, where a factor of the trigonal structure is found equaled to a of hexagonal one divided by $\sqrt{3}$. If comparing now normalized volume of each crystalline structure (Table 1), a relevant swelling of the structure clearly appears for the sample containing Am. The global increase is close to 5 \AA^3 , which is a significant value for lattice modification that confirms the substitution of Am on U site in U_3O_8 oxide.

Table 1. Summarize of the calculated lattice volume for pure U_3O_8 and Am-substituted U_3O_8 .

	Pure U_3O_8		Am-substituted U_3O_8	
	Space group	$C2mm$	$P-62m$	$P-3m1$
Volume (\AA^3)		333.02(2)	169.05(2)	56.33(2)
Normalized volume (\AA^3)		333.02(2)	338.10(2)	337.98(2)

Table 2. Fit parameters obtained after LeBail refinement of the two studied samples.

Phase	Pure U_3O_8		Am-substituted U_3O_8	
	Space group	$C2mm$	$P-62m$	$P-3m1$
GOF		1.44	1.30	1.50
R_p		2.54	2.79	2.82
wR_p		3.48	3.60	3.74

XAS results.*XANES.*

The spectra recorded at the Am L_{III} edge for Am-substituted U₃O₈ and model compounds are presented in Figure 3. The comparison between the sample spectrum and the reference for Am^{+IV} and Am^{+III} clearly shows that Am is totally trivalent in the Am-substituted U₃O₈ structure. Concerning the corresponding U L_{III} edge, spectra (and corresponding derivatives) recorded for pure α -U₃O₈, UO₃ and Am-substituted U₃O₈ are presented in Figure 4. UO₃ corresponds to pure U^{+VI} cation ("yl" like), illustrated by two distinct bands after absorption edge in Figure 4, relevant of two distant U-O distances present: 2.1 Å for apical distance and around 2.38 Å for equatorial distances.^{32,33} For α -U₃O₈ reference, spectrum presents a single significant band after absorption edge, characteristic of the *C2mm* crystallographic structure with similar U-O. The valence of U in UO₃ is +VI while U₃O₈ presents two different U oxidation states (+V and +VI) in order to guarantee the electroneutrality inside the oxide.³⁴ Considering U₃O₈ as stoichiometric oxide at RT, U element is distributed for 33% in U^{+VI} and 66% in U^{+V} for an average valence of 5.33.

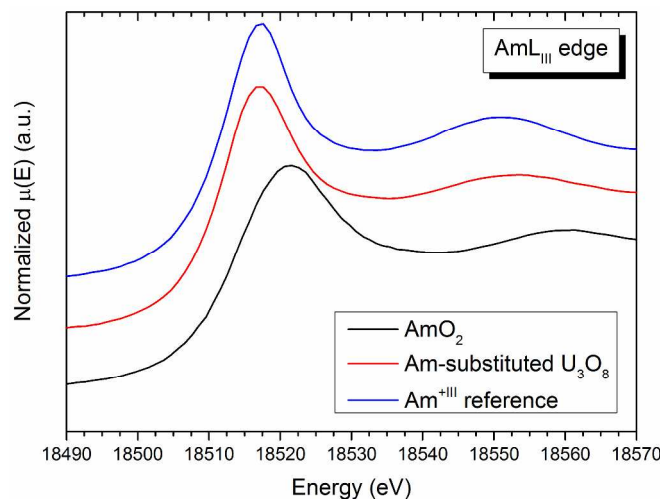


Figure 3. Normalized XANES spectra collected at Am L_{III} edge and 20 K – AmO₂ is in dark grey, Am-substituted U₃O₈ is in blue and the Am^{+III} reference is in red.

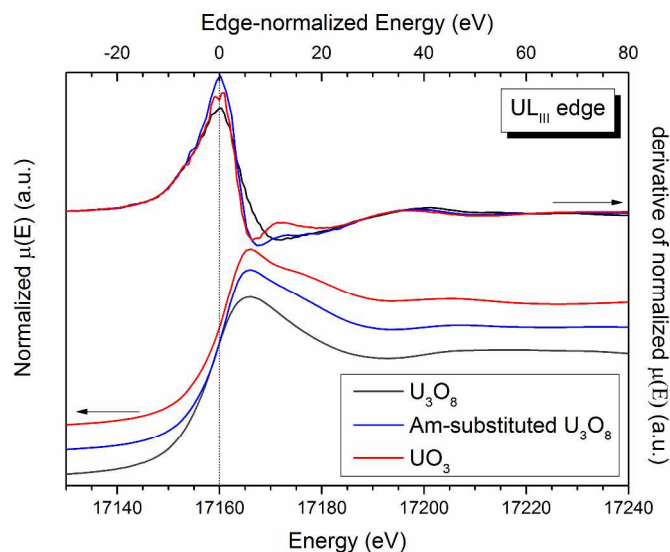


Figure 4. Normalized XANES spectra collected at U L_{III} edge and associated derivatives. 20 K – U₃O₈ is in dark grey, Am-substituted U₃O₈ is in blue and UO₃ is in red.

When looking at Am-substituted U₃O₈ spectrum, it looks intermediary between the two pure uranium oxides. Although it is not as pronounced as for UO₃, two bands are present on the absorption derivative after absorption edge, illustrated by a small shoulder around 17180 eV,

1
2
3 which is completely absent of the U_3O_8 spectrum. This observation would thus be consistent
4
5 with the presence of two different U-O distances in (U,Am)-based oxide approaching the "yl"
6
7 like configuration (as in UO_3). Indeed Figure 4 suggests that U lies in a mixed-valence state with
8
9 unknown +V/+VI. Only high resolution XANES would allow to precisely confirm mixed-
10
11 valence and quantitative proportion of +V and +VI. Indeed, the resolution of the core hole at the
12
13 An $L_{II,III}$ edge (around 7 eV) is far too small to enable such determination with accuracy. One
14
15 can conclude that Am-substituted U_3O_8 XANES derivative (post edge shape) is thus qualitatively
16
17 closer from that of UO_3 than from U_3O_8 . If considering 10 at%. of trivalent Am on +V/VI U
18
19 sites, average U charge for stoichiometric oxide will shift from 5.33 (for pure U_3O_8) to 5.59. This
20
21 would correspond to the presence of 60% of U^{+VI} in the mixed oxide instead of 33% in pure
22
23 U_3O_8 , to compensate trivalent Am presence.
24
25
26
27
28

29 Considering XRD results, previous work validates the hypothesis of substitution, thanks to the
30
31 observed change of crystallographic structures from pure U_3O_8 to Am-substituted U_3O_8 .
32
33 Knowing the oxidation state of Am in the sample (+III), comparison can be made between the
34
35 sizes of the different cations in presence. Considering ionic radius of trivalent Am in hexaedral
36
37 environment equals 1.115 Å for U^{+VI} and 0.87 Å for U^{+V} ,³⁵ it helps to explain the
38
39 global increase of lattice volume with Am-substituted U_3O_8 visible in Table 1.
40
41
42

43 EXAFS study was also performed in order to better understand how the crystalline structure
44
45 accommodates the presence of trivalent Am, what are the close environment of U and Am, and
46
47 what are the differences compared to pure U_3O_8 . This will thus help to confirm possible
48
49 formation of "yl" units.
50
51

52 EXAFS.
53
54
55
56
57
58
59
60

1
2
3 k^2 -weighted EXAFS spectrum and corresponding Fourier transform of pure U_3O_8 are presented
4 in Figure 5 and Figure 6. The best fit structural parameters are summarized in Table 3. For this
5
6 $C2mm$ model structure, fitted distances for single paths are close to crystallographic data.
7
8 Concerning the first U-O axial path, uncertainty is high and the corresponding Debye-Waller
9 factor exhibits a quite high value (0.03 \AA^2). This is due to complicated signal extraction at low k
10 range for this kind of oxides, resulting in large Debye-Waller factors, and high uncertainties for
11 the first shell. Nevertheless, the other distances confirm the correspondence with $C2mm$ space
12 group defined for pure α - U_3O_8 , particularly through sub-cationic lattice and U...U interatomic
13 distances that were fitted until 5.6 \AA .
14
15
16
17
18
19
20
21
22
23

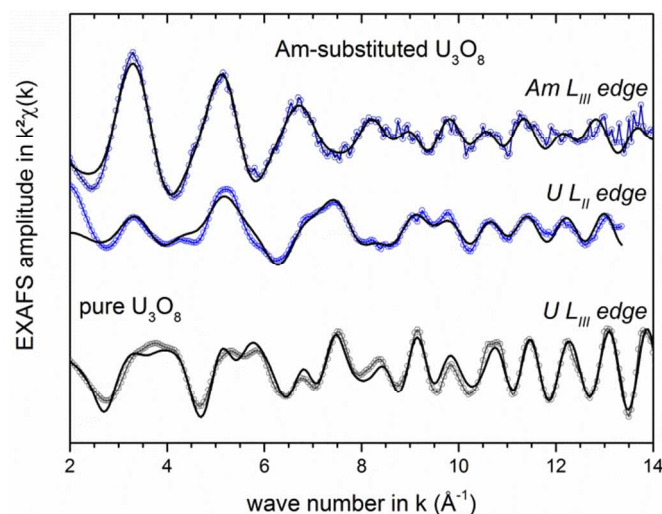


Figure 5. k^2 -weighted EXAFS spectra of the pure U_3O_8 and Am-substituted U_3O_8 . Experimental spectra are plotted in dots (dark grey: pure U_3O_8 at U L_{III} edge; blue and light blue: Am-substituted U_3O_8 at $U L_{II}$ and $Am L_{III}$ edges respectively, adjustments in black lines.

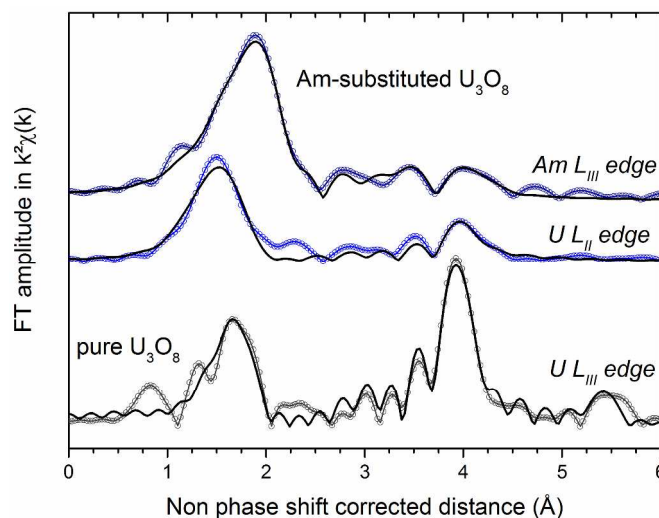


Figure 6. Fourier transform of the EXAFS spectra for pure U_3O_8 and Am-substituted U_3O_8 . Experimental spectra are plotted in dots (dark grey: pure U_3O_8 at U L_{III} edge; blue and light blue: Am-substituted U_3O_8 at $U L_{\text{II}}$ and $Am L_{\text{III}}$ edges respectively, adjustments in black lines).

Considering Am-substituted U_3O_8 , both $P-3m1$ and $P-62m$ space groups were first tested as model references for fitting at the U edge. The trigonal structure did not show good correlation between experimental plot and fit, tending to assess that metal-O and metal...U distances in the sample are closer to the ones identified in the hexagonal reference configuration. Therefore as a starting point for fitting, the path lengths in $P-62m$ structure were considered as model for both Am and U edges.

Focusing on Am environment, Table 3 presents the best fit parameters. XRD previously showed the substitution of Am on U site. Good results obtained for EXAFS spectrum fitting tends to confirm these results, as Am-O and Am...U distances are in good agreement with the ones corresponding to $P-62m$ structure. The increase of interatomic Am-O distances is in agreement with the decrease of formal oxidation state from +5.33 for U in U_3O_8 $C2mm$ to +3 for Am in the present structure, although this is only indicative because both cations don't have the same geometry. Moreover, as $\text{Am}^{\text{+III}}$ has a larger crystal radius (1.115 Å) than U in the same

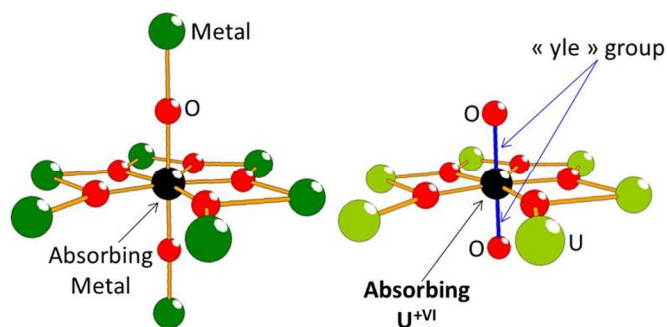
1
2
3 hexahedral configuration (0.87 Å for U^{+VI} and 0.9 Å for U^{+V}),³⁵ it should also contribute to the
4
5 expansion of the O environment. The fit of the Am...U distances was only possible if considering
6
7 an important shortening of the four equatorial Am-U paths, whereas axial distances increase.
8
9 This significant variation, opposing the general tendency of swelling, can be understood if
10
11 anionic and cationic paths are de-correlated. This can be assumed as anionic interatomic
12
13 distances undergo different variations from cationic sublattice, and cations and anions are not
14
15 aligned together on the same direction. It thus renders possible Am...U equatorial distance
16
17 shrinkage, despite swelling of anionic sublattice. On contrary, for the axial direction where Am
18
19 and O are aligned, both Am-O and Am...Am distances increase.
20
21
22
23

24 Fitting U L_{II} EXAFS spectrum for Am-substituted U_3O_8 evidences several structural
25
26 modifications of U closest environment compared to the $P-62m$ structure, summarized in Table
27
28 3. Concerning the U-O single scattering, optimization of the fit led to a split of axial U-O
29
30 distances into two different contributions, with a repartition close to 50/50. The first one equals
31
32 2.03(1) Å and remains very similar to the crystallographic value of 2.07 Å in $P-62m$. The second
33
34 one is found significantly shorter than conventional distance in U_3O_8 , and equals 1.78(1) Å.
35
36 Tentative to remove this short distance or to compensate with a higher Debye Waller value for
37
38 the first shell lead to a very significant degradation of the quality factor ($\Delta\chi^2\nu = 27$ to 265). In
39
40 addition, this result is correlated to the above discussion on XANES spectra, and suggests that
41
42 50(5) % of the U-O bond can be assimilated to "uranyl" as it is very close to uranyl theoretical
43
44 distance (1.76 Å³⁶). As a consequence one may assume that trivalent Am substitution in U_3O_8
45
46 induces structural and charge modifications with an increase of U^{+VI} , as expected with previous
47
48 calculation of charge compensation leading to 60% of U^{+VI} required, instead of 33%. Excess of
49
50 +VI cation thus needs to be organized in the structure through the formation of "uranyl" like
51
52
53
54
55
56
57
58
59
60

1
2
3 units observed by XANES and fitted by EXAFS. Concerning the equatorial U-O distances,
4
5 values determined for the five paths are in agreement with the *P-62m* model: 2.16(1) Å
6
7 compared to 2.21 Å for the four symmetric surrounding O, and 2.62(1) Å compared to 2.67 Å for
8
9 the single one. Focusing now on cationic sublattice, the U...U interatomic distance also reveals
10
11 important modifications with important increase of one distance (+0.16 Å), linked to the four
12
13 equatorial U...U paths, whereas simple axial interatomic distances remain close to
14
15 crystallography. Addition of triple and quadruple scattering paths linked to 2.07 Å U-O axial
16
17 distances considerably improved the quality of the fit. This result strengthens the assumption of
18
19 the coexistence of free uranyl like bonds together with normal U-O axial bonds linked to the sub-
20
21 cationic lattice.
22
23
24
25

26
27 The structural arrangements around U and Am, in pure U₃O₈ and in Am-substituted U₃O₈ are
28
29 thus very different. According to the above data, the Am cation substitutes U and provokes
30
31 general swelling of its close environment except for the Am...U equatorial distances that are
32
33 decreased. The U and O atoms of the Am equatorial plane are not aligned, and make possible
34
35 this Am...U distance modification. This is also evidenced by the U...U distortion caused by the
36
37 presence of Am with different structural constraints on cationic and anionic sublattices. The
38
39 major adjustment to the *P-62m* structure comes from the necessity to add to the system shorter
40
41 free U-O bonds which would be related to axial uranyl like units, as illustrated in Figure 7.
42
43 Scheme thus shows the two kinds of cationic and anionic environment around U and Am. The
44
45 left part shows *P-62m* configuration taken by Am and 50% of U, mostly U^{+V}, besides distance
46
47 distortion. Green atoms correspond to U or Am cations around absorbing cation, whereas red
48
49 ones are O. The right configuration illustrates the environment determined with free “yle” units
50
51 around U, attributed to U^{+VI}, identified with the two blue double U=O bonds. As a conclusion,
52
53
54
55
56
57
58
59
60

1
2
3 from U environment, anionic sublattice undergoes the major part of structural changes through
4
5 free uranyl double bonds formation induced by a higher amount of U^{+VI} in the mixed oxide, to
6
7 compensate Am^{+III} presence. As U_3O_8 oxides have planar disposition, this specific configuration
8
9 enables to presume that it favors alternating uranyl planes with conventional U^{+V} $P-62m$ planes.
10
11



12
13
14
15
16
17
18
19
20
21
22
23
24
25 Figure 7. (left) First anionic and cationic coordination shells for $P-62m$ space group used for
26
27 EXAFS fitting. (right) First anionic and cationic coordination shells for U^{+VI} , involving “yle”
28
29 configuration - Green atoms correspond to metals (U, Am), light green atoms to U, red ones to
30
31 O. Black atom is considered as absorbing atom. Orange bond are simple and blue ones are
32
33 double.
34
35
36
37
38
39
40
41
42
43
44
45
46
47
48
49
50
51
52
53
54
55
56
57
58
59
60

Table 3. EXAFS data on pure U_3O_8 and Am-substituted U_3O_8 , and comparison with theory. S_0^2 is the EXAFS global amplitude factor, Δe_0 is the energy threshold, ϵ is the average noise and R_{factor} is the agreement factor of the fit. Numbers in round brackets are uncertainties.

		Bond type	Distance (Å)	crystallography ref (Å)	σ^2 (Å ²)	
Pure U_3O_8 reference <i>C2mm</i>	$R_{\text{factor}} = 3.1\%$ $\Delta\chi^2_v = 0.57$ $S_0^2 = 0.8$ $\Delta e_0 = 5.85$ $\epsilon = 0.004$	2 axial U-O	1.99(5)	2.07	0.0301	
		U L_{III} edge	4 equatorial U-O	2.21(1)	2.16	0.0077
		1 equatorial U-O	2.59(1)	2.54	0.0237	
		2 equatorial U...U	3.70(1)	3.74	0.0084	
		2 equatorial U...U	3.84(1)	3.88	0.0138	
		2 equatorial U...U	4.14(1)	4.18	0.0065	
		2 axial U...U	4.16(1)	4.15	0.0065	
		8 diagonal U...U	5.62(1)	5.59	0.0070	
Am-substituted U_3O_8	$R_{\text{factor}} = 3.6\%$ $\Delta\chi^2_v = 27.48$ $S_0^2 = 0.9$ $\Delta e_0 = -4.77$ $\epsilon = 0.003$	U L_{II} edge	(50%) 2 axial U-O	2.03(1)	2.07	0.0165
		(50%) 2 axial U=O'	1.78(1)	2.07	0.0036	
		4 equatorial U-O	2.16(1)	2.21	0.0085	
		1 equatorial U-O	2.62(1)	2.67	0.0159	
		6 equatorial U-U	4.01(2)	3.83	0.0137	
		(50%) 2 axial U-U	4.17(1)	4.14	0.0015	
		Am L_{III} edge	2 axial Am-O	2.26(1)	2.07	0.0033
		4 equatorial Am-O	2.46(2)	2.21	0.0032	
		1 equatorial Am-O	2.93(2)	2.68	0.0022	
		6 equatorial Am-U	3.69(2)	3.83	0.0178	
	$R_{\text{factor}} = 7.7\%$ $\Delta\chi^2_v = 4.56$ $S_0^2 = 1.0$ $\Delta e_0 = 6.02$ $\epsilon = 0.012$	2 axial Am-U	4.27(2)	4.15	0.0028	

CONCLUSION

These experiments have investigated for the first time the possibility for trivalent Am to be substituted in α -U₃O₈ structure. Combination of XRD and XAS experiments led to the conclusion that substitution is possible thanks to structure accommodation, through transformation from initial orthorhombic to hexagonal structure for Am-substituted oxide. The latter, corresponding to *P-62m* space group, owns a single cationic site, increasing the global symmetry of the structure, but also attesting of a higher metallic disorder. The global cationic charge order of orthorhombic structure (*C2mm* space group), where U^{+V} and U^{+VI} get their own metallic site, is broken by the presence of trivalent Am, leading to space group change. Focusing on close environment of U and Am in the mixed-oxide determined through EXAFS analysis, Am is well-fitted with distances characteristic of hexagonal structure, but causes general increase of interatomic distances around it. U is suffering from more structural rearrangements with the formation of "yl" like bonds, resulting in structural re-organization of U^{+VI} in uranyl units, whose quantity is increased to 60% instead of 33% to compensate trivalent Am presence. Planar geometry of U₃O₈-type oxides suggests alternating planes of U^{+VI} with uranyl units, and U^{+V} in conventional *P-62m* configuration. These results are first new insights on the possibility for U₃O₈ to accommodate, when submitted to high stress such as substitution of trivalent actinide, and propose first solutions for structural arrangements.

AUTHOR INFORMATION

Corresponding Author

* Dr. Thibaud Delahaye: thibaud.delahaye@cea.fr ; 0033466796542 – CEA, DEN,

DRCP/SERA/LCAR, F-30207 Bagnols-sur-Cèze Cedex, France

ACKNOWLEDGMENT

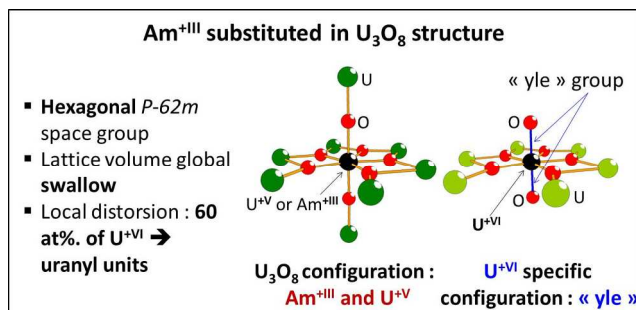
The authors would like to thank F. Boucher for his precious advices on oxide structures. They also thank M. Bataille and P. Coste for sample preparation; A. Gauthé, I. Jobelin, P. Grangaud and J.-M. Pomarède for sample synthesis. We acknowledge the ESRF Synchrotron Light Source for provision of beamtime at the ROBL beamline and P. Colomp for sample transportation. M. Caisso is grateful for Ph.D. fellowship funding by the CEA PACFA program.

REFERENCES

- (1) McEachern, R. J.; Taylor, P. *J. Nucl. Mater.* **1998**, *254* (2–3), 87–121.
- (2) Gras, J.-M.; Quang, R. D.; Masson, H.; Lieven, T.; Ferry, C.; Poinssot, C.; Debes, M.; Delbecq, J.-M. *J. Nucl. Mater.* **2007**, *362* (2–3), 383–394.
- (3) Ferry, C.; Poinssot, C.; Cappelaere, C.; Desgranges, L.; Jegou, C.; Miserque, F.; Piron, J. P.; Roudil, D.; Gras, J. M. *J. Nucl. Mater.* **2006**, *352* (1–3), 246–253.
- (4) Thomas, L. E.; Einziger, R. E.; Buchanan, H. C. *J. Nucl. Mater.* **1993**, *201*, 310–319.
- (5) Warin, D. *J. Nucl. Sci. Technol.* **2007**, *44* (3), 410–414.
- (6) Delahaye, T.; Lebreton, F.; Horlait, D.; Herlet, N.; Dehaut, P. *J. Nucl. Mater.* **2013**, *432* (1–3), 305–312.
- (7) Bejaoui, S. In *Proceedings of GLOBAL 2011*; Makuhari, Japan, 2011.
- (8) Haas, D. *MOX fuel fabrication experience at Belgonucleaire*; Technical committee meeting on recycling of plutonium and uranium in water reactor fuel; International Atomic Energy Agency: Vienna (Austria), 1997.
- (9) Baron, D. D.; Hallstadius, L. In *Comprehensive Nuclear Materials*; Konings, R. J. M., Ed.; Elsevier: Oxford, 2012; pp 481–514.
- (10) Andresen, A. F. *Acta Crystallogr.* **1958**, *11* (9), 612–614.
- (11) Ball, R. G. J.; Dickens, P. G. *J. Mater. Chem.* **1991**, *1* (1), 105–112.
- (12) Loopstra, B. O. *Acta Crystallogr.* **1964**, *17* (6), 651–654.
- (13) Wen, X.-D.; Martin, R. L.; Scuseria, G. E.; Rudin, S. P.; Batista, E. R.; Burrell, A. K. *J. Phys. Condens. Matter* **2013**, *25* (2), 25501.
- (14) Loopstra, B. O. *J. Appl. Crystallogr.* **1970**, *3* (2), 94–96.
- (15) Ackermann, R. J.; Chang, A. T.; Sorrell, C. A. *J. Inorg. Nucl. Chem.* **1977**, *39* (1), 75–85.
- (16) Loopstra, B. O. *Acta Crystallogr. B* **1970**, *26* (5), 656–657.
- (17) Desgranges, L.; Palancher, H.; Gamaléri, M.; Micha, J. S.; Optasanu, V.; Raceanu, L.; Montesin, T.; Creton, N. *J. Nucl. Mater.* **2010**, *402* (2–3), 167–172.
- (18) Benedict, U. *J. Nucl. Mater.* **1970**, *35* (3), 356–361.
- (19) Finch, R. J.; Jeremy Kropf, A. *MRS Online Proc. Libr.* **2002**, *757*, null-null.
- (20) Remy, E. Étude de la synthèse de sphères d'oxyde d'actinides et/ou de lanthanides et de leur aptitude à la céramisation, Université de Montpellier 2, 2013.
- (21) Remy, E.; Picart, S.; Delahaye, T.; Jobelin, I.; Dugne, O.; Bisel, I.; Blanchart, P.; Ayrat, A. *J. Nucl. Mater.* **2014**, *448* (1–3), 80–86.

- 1
2
3
4 (22) Remy, E.; Picart, S.; Delahaye, T.; Jobelin, I.; Lebreton, F.; Horlait, D.; Bisel, I.;
5 Blanchart, P.; Ayrat, A. *J. Nucl. Mater.* **2014**, *453* (1–3), 214–219.
6 (23) Caisso, M.; Picart, S.; Belin, R. C.; Lebreton, F.; Martin, P. M.; Dardenne, K.; Rothe, J.;
7 Neuville, D. R.; Delahaye, T.; Ayrat, A. *Dalton Trans.* **2015**, *44* (14), 6391–6399.
8 (24) Carjaval, J. R. *Satell. Meet. Powder Diffr. XVIUCr Congr.* **1990**.
9 (25) Rodríguez-Carvajal, J. *Phys. B Condens. Matter* **1993**, *192* (1–2), 55–69.
10 (26) Le Bail, A. *Powder Diffr.* **2005**, *20* (4), 316–326.
11 (27) Newville, M. *J. Synchrotron Radiat.* **2001**, *8* (2), 322–324.
12 (28) Ravel, B.; Newville, M. *J. Synchrotron Radiat.* **2005**, *12* (4), 537–541.
13 (29) Rehr, J. J.; Kas, J. J.; Vila, F. D.; Prange, M. P.; Jorissen, K. *Phys. Chem. Chem. Phys.*
14 *PCCP* **2010**, *12* (21), 5503–5513.
15 (30) Arab-Chapelet, B.; Martin, P.; Costenoble, S.; Delahaye, T.; Scheinost, A. C.; Grandjean,
16 S.; Abraham, F. *Dalton Trans.* **2016**.
17 (31) Hoekstra, H. R.; Siegel, S.; Fuchs, L. H.; Katz, J. J. *J. Phys. Chem.* **1955**, *59* (2), 136–138.
18 (32) Siegel, S.; Hoekstra, H. R. *Inorg. Nucl. Chem. Lett.* **1971**, *7* (6), 497–504.
19 (33) Greaves, C.; Fender, B. E. F. *Acta Crystallogr. B* **1972**, *28* (12), 3609–3614.
20 (34) Kvashnina, K. O.; Butorin, S. M.; Martin, P.; Glatzel, P. *Phys. Rev. Lett.* **2013**, *111* (25),
21 253002.
22 (35) Shannon, R. D. *Acta Crystallogr. Sect. A* **1976**, *32* (5), 751–767.
23 (36) Jones, L. H. *Spectrochim. Acta* **1959**, *15*, 409–411.
24
25
26
27
28
29
30
31
32
33
34
35
36
37
38
39
40
41
42
43
44
45
46
47
48
49
50
51
52
53
54
55
56
57
58
59
60

For table of contents only.



This paper presents first assumption for trivalent Am substitution in U₃O₈ structure. Structural properties of this unknown mixed oxide are presented for first time through combination of XRD, XANES and EXAFS measurements.